Inorganic Chemistry

ARTICLE

pubs.acs.org/IC

Ternary Rare-Earth Arsenides $REZn_3As_3$ (RE = La−Nd, Sm) and $RECd_3As_3$ (RE = La−Pr)

Stanislav S. Stoyko and Arthur Mar*

Department of Chemistry, University of Alberta, Edmonton, Alberta, Canada T6G 2G2

Supporting Information

ABSTRACT: Ternary rare-earth zinc arsenides $REZn_3As_3$ (RE = La−Nd, Sm) with polymorphic modifications different from the previously known defect $CaAl_2Si_2$-type forms, and the corresponding rare-earth cadmium arsenides $RECd_3As_3$ (RE = La−Pr), have been prepared by reaction of the elements at 800 °C. $LaZn_3As_3$ adopts a new orthorhombic structure type (Pearson symbol *oP*28, space group *Pnma*, $Z = 4$, $a = 12.5935(8)$ Å, $b = 4.1054(3)$ Å, $c = 11.5968(7)$ Å) in which $ZnAs_4$ tetrahedra share edges to form ribbons that are fragments of other layered arsenide structures; these ribbons are then interconnected in a three-dimensional framework with large channels aligned parallel to the *b* direction that are occupied by La^{3+} cations. All remaining compounds adopt the hexagonal $ScAl_3C_3$-type structure (Pearson symbol *hP*14, space group $P6_3/mmc$, $Z = 2$; $a = 4.1772(7)-4.1501(2)$ Å, $c = 20.477(3)-20.357(1)$ Å for $REZn_3As_3$ (RE = Ce, Pr, Nd, Sm); $a = 4.4190(3)-4.3923(2)$ Å, $c = 21.4407(13)-21.3004(8)$ Å for $RECd_3As_3$ (RE = La−Pr)) in which $[M_3As_3]^{3-}$ layers (M = Zn, Cd), formed by a triple stacking of nets of close-packed As atoms with M atoms occupying tetrahedral and trigonal planar sites, are separated by La^{3+} cations. Electrical resistivity measurements and band structure calculations revealed that orthorhombic $LaZn_3As_3$ is a narrow band gap semiconductor.

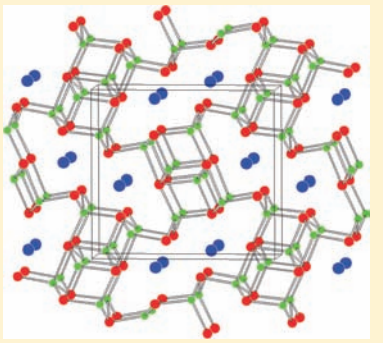

INTRODUCTION

The exciting discovery of arsenide-based superconductors such as $BaFe_2As_2$ and LaFeAsO provides the impetus for more systematic investigation of ternary and quaternary arsenides.[1,2] Ternary rare-earth transition-metal arsenides RE−M−As remain few compared to the phosphides or antimonides, and their structures and properties cannot be easily extrapolated from either. For example, $RE_{12}Fe_{57.5}As_{41}$ (RE = La, Ce) is a unique metal-rich phase not formed for the corresponding phosphide or antimonide.[3] Where series of isostructural pnictides do exist, such as $REZn_{1-x}Pn_2$ (Pn = As, Sb, Bi) with the defect $HfCuSi_2$-type structure, the extent of RE substitution and the degree of substoichiometry can be understood in terms of size and electronic effects as the pnicogen is varied.[4−7] In the course of examining the homogeneity range in one of these phases, $SmZn_{1-x}As_2$, we identified the existence of a new ternary phase, $SmZn_3As_3$.[5] Surprisingly, it does not belong to the recently reported series $RE_{0.67}Zn_2As_2$ (RE = La−Nd, Sm), which has an identical composition (when the formula is multiplied by 3/2) but a different structure (defect $CaAl_2Si_2$-type).[8] We describe here the preparation of the arsenides $REZn_3As_3$ (RE = La−Nd, Sm) and $RECd_3As_3$ (RE = La−Pr), and their structural relationships. In particular, $LaZn_3As_3$ was found to adopt a new polymorphic modification with a unique structure type that resembles that of $CaFe_4As_3$[9−11] and contains fragments of the $BaFe_2As_2$ and LaFeAsO structures. The electronic structure of $LaZn_3As_3$ was evaluated through band structure calculations and electrical resistivity measurements.

EXPERIMENTAL SECTION

Synthesis. The ternary phase $SmZn_3As_3$ was first identified during experiments to determine the homogeneity range in $SmZn_{1-x}As_2$.[5] Investigation of other rare-earth and transition metal substitutions led to the preparation of the series $REZn_3As_3$ and $RECd_3As_3$. Mixtures of freshly filed pieces of various RE metals (99.9%, Hefa), Zn shot (99.99%, Aldrich) or Cd shot (99.95%, Alfa-Aesar), and As lumps (99.999%, Alfa-Aesar) on a 0.3 g scale in a molar ratio of 1:3:3 were placed within sealed evacuated fused-silica tubes. The tubes were heated at 500 °C for 2 days, heated to 800 °C over 1 day, held at this temperature for 7 days, and then cooled to room temperature over 2 days. The products were analyzed by their powder X-ray diffraction (XRD) patterns, collected on an Inel powder diffractometer (Cu $K\alpha_1$ radiation) equipped with a CPS 120 detector. $LaZn_3As_3$ (own type) could be obtained in the form of quantitatively pure powder by this procedure. Needle-shaped single crystals of $LaZn_3As_3$ were grown by heating this phase-pure powder sample at 900 °C for 7 days followed by slow-cooling to room temperature over 2 days. The remaining samples contained $REZn_3As_3$ (RE = Ce−Nd, Sm) and $RECd_3As_3$ (RE = La−Pr) ($ScAl_3C_3$-type) as the major phase, but also minor amounts of other binary phases because of deviations in reaction stoichiometry caused by the formation of intermediate Zn_3As_2 or Cd_3As_2 phases,[12−14] which tended to sublimate at the top of the tubes. Therefore, the as-prepared samples (including the sublimed Zn_3As_2 or Cd_3As_2) were reground and further annealed at 800 °C for 7 days in the presence of a few milligrams of I_2 added as a mineralizing agent. Pure samples of $REZn_3As_3$ or $RECd_3As_3$ ($ScAl_3C_3$-type) were

Received: August 5, 2011
Published: September 27, 2011

dx.doi.org/10.1021/ic201708x | *Inorg. Chem.* 2011, 50, 11152–11161

Table 1. Cell Parameters for $REZn_3As_3$ (RE = La−Nd, Sm) and $RECd_3As_3$ (RE = La−Pr) [a]

compound	a (Å)	b (Å)	c (Å)	V/Z (Å^3)
$LaZn_3As_3$	12.589(2)	4.1032(5)	11.596(2)	149.7(1)
$CeZn_3As_3$	4.1772(7)	4.1772(7)	20.477(3)	154.7(1)
$PrZn_3As_3$	4.1699(4)	4.1699(4)	20.445(2)	153.9(1)
$NdZn_3As_3$	4.1616(5)	4.1616(5)	20.407(2)	153.1(1)
$SmZn_3As_3$	4.1462(4)	4.1462(4)	20.335(2)	151.4(1)
$LaCd_3As_3$	4.4159(6)	4.4159(6)	21.441(3)	181.1(1)
$CeCd_3As_3$	4.4014(4)	4.4014(4)	21.344(3)	179.1(1)
$PrCd_3As_3$	4.3885(6)	4.3885(6)	21.292(3)	177.6(1)

[a] Refined from powder X-ray diffraction data.

obtained in the form of hexagonal plate-shaped single crystals. (This procedure is equally successful for the growth of $LaZn_3As_3$ single crystals.) Energy-dispersive X-ray (EDX) analysis with a Zeiss EVO MA 15 scanning electron microscope (SEM) on these crystals revealed chemical compositions (14(1)% RE, 43(2)% Zn, 43(2)% As for $REZn_3As_3$; 13(1)% RE, 44(2)% Cd, 43(2)% As for $RECd_3As_3$) that agree well with expectations (14% RE, 43% Zn or Cd, 43% As). Syntheses of heavier trivalent rare-earth members were attempted for $REZn_3As_3$ (RE = Gd−Tm, Lu) and $RECd_3As_3$ (RE = Nd, Sm, Gd−Tm, Lu) under similar conditions, but they resulted only in the formation of binary arsenide (RE−As; Zn−As or Cd−As) phases.

Unit cell parameters refined from the powder XRD patterns (Figures S1 and S2 in the Supporting Information) are listed in Table 1. Representative SEM micrographs of needle-shaped crystals of $LaZn_3As_3$ and hexagonal plate-shaped crystals of $SmZn_3As_3$ are shown in Figure S3 in the Supporting Information.

Structure Determination. Suitable crystals were available for most $REZn_3As_3$ and $RECd_3As_3$ samples prepared, except for $CeZn_3As_3$, for which the crystal quality was inexplicably poor. (All crystals of $CeZn_3As_3$ examined on the diffractometer revealed very streaky reflection profiles. A Rietveld refinement was also attempted for $CeZn_3As_3$ but was complicated by severe preferred orientation effects evident in the powder XRD pattern and difficulties in fitting the peak profiles.) Single-crystal intensity data were collected at room temperature on a Bruker D8/SMART APEX II CCD diffractometer using ω scans. Data were acquired in 5−6 batch sets with a frame width of 0.3° in ω and an exposure time of 20 s per frame. Structure solution and refinement were carried out with use of the SHELXTL (version 6.12) program package.[15] Face-indexed numerical absorption corrections were applied. Crystal data and further details of the data collection are given in Table 2.

For $LaZn_3As_3$, the Laue symmetry, systematic absences, and intensity statistics favored the centrosymmetric orthorhombic space group *Pnma*. Initial positions for all atoms were easily located by direct methods. Refinements proceeded smoothly, leading to excellent agreement factors, unremarkable displacement parameters, and a clean difference electron density map.

For the remaining $REZn_3As_3$ (RE = Pr, Nd, Sm) and $RECd_3As_3$ (RE = La−Pr) crystals, which clearly exhibit hexagonal habits, the space group $P6_3/mmc$ was chosen on the basis that the powder XRD patterns match well with the known $ScAl_3C_3$-type structure.[16] Initial atomic positions were taken from the structure of $PrZn_3P_3$.[17] Refinement of this model in $P6_3/mmc$ led to large displacement parameters at the 2*c* (1/3, 2/3, 1/4) site occupied by M2 (M = Zn, Cd) atoms and at the 2*d* site (1/3, 2/3, 3/4) occupied by As2 atoms. All $ScAl_3C_3$-type structures reported thus far exhibit unusually pronounced displacements along the *c* direction for the atoms in these sites;[16−20] this pathological feature has normally been treated by splitting these atomic sites, refining in lower symmetry space groups (such as $P6_322$ or $P6_3mc$), invoking merohedral twinning, or some combination of these procedures. The classic structure determinations of covellite (CuS), whose relationship to the $ScAl_3C_3$-type structure is mentioned later, pose many of the same problems.[21−23] However, in the arsenides presented here, there are also significant displacements within the *ab* plane such that the ellipsoids are highly oblate (U_{11}, $U_{22} > U_{33}$). Attempts were made to refine models within the numerous subgroups of $P6_3/mmc$ as well as lower-symmetry Laue groups, to no avail. An acceptable model that describes the average structure through a minimum number of refinable parameters is one in which the M2 and As2 atoms are each placed in 6*h* sites (x, $2x$, 1/4), lying off the $\bar{6}$ axis but still on a mirror plane normal to *c* (site symmetry *mm*2), with fixed occupancy factors of 1/3 within space group $P6_3/mmc$. When this model was refined, the displacement parameters for the M2 and As2 atoms were reduced to more reasonable values. The displacement ellipsoids were now fairly isotropic for the As2 atoms. However, the M2 atoms still had somewhat high U_{33} values, leading to slightly prolate ellipsoids along the *c* direction; in other words, we reverted to the normal situation seen in $ScAl_3C_3$-type structures, for which the usual strategies mentioned above could be applied. Further splitting of these M2 sites so that they are displaced off the mirror plane normal to *c* did not lead to improvements. This is suggestive of dynamic disorder, as supported by a structure determination of $PrZn_3As_3$ at low temperatures (173 K), in which the Zn2 atom remains on the mirror plane but with a lower U_{33} value, indicating reduced vibrational motion along the *c* direction. Refinement results for the structure of $PrZn_3As_3$ in space groups $P6_3/mmc$ (room and low temperature), $P6_322$, and $P6_3mc$ are compared in Table S1 in the Supporting Information. Lowering the space group symmetry led to improvements in the agreement factors but at the expense of nearly doubling the number of parameters (cf., $R(F)$ = 0.075, n_p = 18 in $P6_3/mmc$ vs $R(F)$ = 0.062, n_p = 30 in $P6_3mc$). We opt to report the model in $P6_3/mmc$ in the interest of simplifying subsequent discussion, keeping in mind that an average structure is being described.

Atomic positions were standardized with the program STRUCTURE TIDY.[24] Final values of the positional and displacement parameters are given in Table 3, and selected interatomic distances are listed in Tables 4 and 5. Further data, in the form of crystallographic information files (CIFs), are available as Supporting Information or may be obtained from Fachinformationszentrum Karlsruhe, Abt. PROKA, 76344 Eggenstein-Leopoldshafen, Germany (No. 423591 to 423597).

Physical Property Measurements. The long (>1 mm) single crystals of $LaZn_3As_3$ were suitable for electrical resistivity measurements, which were made along the needle axis (corresponding to the crystallographic *b* axis) between 2 and 300 K by standard four-probe techniques on a Quantum Design Physical Property Measurement System (PPMS) equipped with an AC transport controller (Model 7100). The current was 100 μA, and the frequency was 16 Hz.

Measurements of DC magnetic susceptibility were made on powders of $REZn_3As_3$ (RE = La, Ce, Pr, Nd) under an applied field of 0.5 T on a Quantum Design 9T-PPMS DC magnetometer/AC susceptometer. Susceptibility values were corrected for contributions from the holder and sample diamagnetism.

Band Structure Calculations. Tight-binding linear muffin tin orbital band structure calculations were performed with use of the Stuttgart TB-LMTO program[25] on $LaZn_3As_3$ with three models: (i) orthorhombic, (ii) trigonal, and (iii) hexagonal. The orthorhombic model is based on $LaZn_3As_3$ (own type) in space group *Pnma*, with cell parameters and atomic positions taken from the experimental crystal structure reported here. The trigonal model is based on a $\sqrt{3}a \times \sqrt{3}a \times 2c$ superstructure of the defect $CaAl_2Si_2$-type structure adopted by $La_{0.67}Zn_2As_2$ in which the 2/3 occupancy of the rare-earth atoms within close-packed triangular nets (3^6 in Schläfli notation) is distributed to give ordered honeycomb nets (6^3), which are then arranged in an AB stacking sequence.[8] The cell parameters (a' = 7.240 Å, c' = 14.186 Å) were derived from the experimental subcell of $La_{0.67}Zn_2As_2$, and the

dx.doi.org/10.1021/ic201708x |*Inorg. Chem.* 2011, 50, 11152–11161

Table 2. Crystallographic Data for $REZn_3As_3$ (RE = La, Pr, Nd, Sm) and $RECd_3As_3$ (RE = La−Pr)

formula	$LaZn_3As_3$	$PrZn_3As_3$	$NdZn_3As_3$	$SmZn_3As_3$
formula mass (amu)	559.78	561.78	565.11	571.22
space group	*Pnma* (No. 62)	$P6_3/mmc$ (No. 194)	$P6_3/mmc$ (No. 194)	$P6_3/mmc$ (No. 194)
a (Å)	12.5935(8)	4.1709(2)	4.1655(2)	4.1501(2)
b (Å)	4.1054(3)	4.1709(2)	4.1655(2)	4.1501(2)
c (Å)	11.5968(7)	20.4429(10)	20.4267(9)	20.3570(8)
V (Å^3)	599.57(7)	307.99(3)	306.95(2)	303.64(2)
Z	4	2	2	2
ρ_{calcd} (g cm^{-3})	6.201	6.058	6.114	6.248
cryst dimensions (mm)	0.10 × 0.13 × 0.15	0.04 × 0.14 × 0.16	0.06 × 0.13 × 0.19	0.03 × 0.09 × 0.15
radiation	graphite-monochromated Mo Kα, λ = 0.71073 Å			
μ(Mo Kα) (mm^{-1})	35.12	35.16	35.80	37.31
transmission factors	0.055−0.148	0.048−0.356	0.036−0.342	0.056−0.522
2θ limits	4.78−66.22°	3.98−65.86°	3.98−65.94°	4.00−66.22°
data collected	$-19 \le h \le 18$	$-6 \le h \le 6$	$-6 \le h \le 6$	$-6 \le h \le 6$
	$-6 \le k \le 6$	$-6 \le k \le 6$	$-6 \le k \le 6$	$-6 \le k \le 6$
	$-17 \le l \le 17$	$-31 \le l \le 30$	$-31 \le l \le 30$	$-30 \le l \le 30$
no. of data collected	7872	3720	3864	3869
no. of unique data, including $F_o^2 < 0$	1256 (R_{int} = 0.018)	273 (R_{int} = 0.055)	272 (R_{int} = 0.025)	272 (R_{int} = 0.037)
no. of unique data, with $F_o^2 > 2\sigma(F_o^2)$	1228	273	272	270
no. of variables	44	18	18	18
$R(F)$ for $F_o^2 > 2\sigma(F_o^2)$ [a]	0.016	0.075	0.074	0.074
$R_w(F_o^2)$ [b]	0.034	0.192	0.193	0.192
goodness of fit	1.27	1.39	1.48	1.50
$(\Delta\rho)_{max}$, $(\Delta\rho)_{min}$ (e Å^{-3})	0.96, −1.02	4.46, −3.98	5.44, −4.60	5.28, −4.66

formula	$LaCd_3As_3$	$CeCd_3As_3$	$PrCd_3As_3$
formula mass (amu)	700.87	702.08	702.87
space group	$P6_3/mmc$ (No. 194)	$P6_3/mmc$ (No. 194)	$P6_3/mmc$ (No. 194)
a (Å)	4.4190(3)	4.4050(1)	4.3923(2)
b (Å)	4.4190(3)	4.4050(1)	4.3923(2)
c (Å)	21.4407(13)	21.3511(7)	21.3004(8)
V (Å^3)	362.59(4)	358.79(2)	355.88(3)
Z	2	2	2
ρ_{calcd} (g cm^{-3})	6.419	6.499	6.559
cryst dimensions (mm)	0.04 × 0.10 × 0.13	0.03 × 0.17 × 0.20	0.02 × 0.11 × 0.11
radiation	graphite monochromated Mo Kα, λ = 0.71073 Å		
μ(Mo Kα) (mm^{-1})	27.91	28.60	29.28
transmission factors	0.114−0.454	0.038−0.508	0.188−0.566
2θ limits	3.80−66.14°	3.82−66.44°	3.82−66.72°
data collected	$-6 \le h \le 6$	$-6 \le h \le 6$	$-6 \le h \le 6$
	$-6 \le k \le 6$	$-6 \le k \le 6$	$-6 \le k \le 6$
	$-32 \le l \le 32$	$-32 \le l \le 32$	$-32 \le l \le 32$
no. of data collected	4613	4592	4689
no. of unique data, including $F_o^2 < 0$	317 (R_{int} = 0.082)	316 (R_{int} = 0.058)	318 (R_{int} = 0.056)
no. of unique data, with $F_o^2 > 2\sigma(F_o^2)$	305	315	305
no. of variables	18	18	18
$R(F)$ for $F_o^2 > 2\sigma(F_o^2)$ [a]	0.078	0.073	0.067
$R_w(F_o^2)$ [b]	0.226	0.212	0.177
goodness of fit	1.25	1.34	1.40
$(\Delta\rho)_{max}$, $(\Delta\rho)_{min}$ (e Å^{-3})	6.48, −4.15	6.24, −4.42	5.97, −4.50

[a] $R(F) = \Sigma||F_o| - |F_c||/\Sigma|F_o|$. [b] $R_w(F_o^2) = [\Sigma[w(F_o^2 - F_c^2)^2]/\Sigma wF_o^4]^{1/2}$; $w^{-1} = [\sigma^2(F_o^2) + (Ap)^2 + Bp]$, where $p = [\max(F_o^2,0) + 2F_c^2]/3$.

atomic positions were derived from the crystal structure of $Ce_{0.67}Zn_2As_2$.[8] This ordered superstructure, with atomic positions La1 in 2*a* (0, 0, 1/4), La2 in 2*c* (1/3, 2/3, 1/4), Zn in 12*i* (1/3, 0, 0.0662), and As in 12*i* (1/3, 0, −0.1202) in space group $P\bar{3}1c$ (no. 163), has the same number

dx.doi.org/10.1021/ic201708x |*Inorg. Chem.* 2011, 50, 11152–11161

Table 3. Atomic Coordinates and Equivalent Isotropic Displacement Parameters for $REZn_3As_3$ (RE = La, Pr, Nd, Sm) and $RECd_3As_3$ (RE = La−Pr)

atom	Wyckoff position	x	y	z	U_{eq} (Å^2)[a]
		$LaZn_3As_3$			
La	4*c*	0.33744(2)	1/4	0.94114(2)	0.01134(5)
Zn1	4*c*	0.06718(3)	1/4	0.03856(4)	0.01375(8)
Zn2	4*c*	0.27666(3)	1/4	0.65419(4)	0.01440(9)
Zn3	4*c*	0.44741(3)	1/4	0.23536(4)	0.01444(9)
As1	4*c*	0.08360(3)	1/4	0.61627(3)	0.01015(7)
As2	4*c*	0.14692(3)	1/4	0.23923(3)	0.01013(7)
As3	4*c*	0.36050(3)	1/4	0.43440(3)	0.01079(7)
		$PrZn_3As_3$			
Pr	2*a*	0	0	0	0.0111(8)
Zn1	4*f*	1/3	2/3	0.6308(2)	0.0160(11)
Zn2[b]	6*h*	0.269(2)	0.538(4)	1/4	0.027(3)
As1	4*f*	1/3	2/3	0.0871(2)	0.0111(9)
As2[b]	6*h*	0.601(2)	0.202(3)	1/4	0.012(2)
		$NdZn_3As_3$			
Nd	2*a*	0	0	0	0.0107(7)
Zn1	4*f*	1/3	2/3	0.6306(2)	0.0157(11)
Zn2[b]	6*h*	0.267(2)	0.534(4)	1/4	0.027(3)
As1	4*f*	1/3	2/3	0.0866(2)	0.0108(9)
As2[b]	6*h*	0.602(2)	0.204(3)	1/4	0.011(2)
		$SmZn_3As_3$			
Sm	2*a*	0	0	0	0.0108(8)
Zn1	4*f*	1/3	2/3	0.6301(2)	0.0155(11)
Zn2[b]	6*h*	0.267(2)	0.533(4)	1/4	0.027(3)
As1	4*f*	1/3	2/3	0.0854(2)	0.0108(9)
As2[b]	6*h*	0.603(2)	0.207(3)	1/4	0.011(2)
		$LaCd_3As_3$			
La	2*a*	0	0	0	0.0144(7)
Cd1	4*f*	1/3	2/3	0.6283(1)	0.0203(8)
Cd2[b]	6*h*	0.265(2)	0.530(3)	1/4	0.044(2)
As1	4*f*	1/3	2/3	0.0802(2)	0.0143(9)
As2[b]	6*h*	0.600(2)	0.199(3)	1/4	0.022(2)
		$CeCd_3As_3$			
Ce	2*a*	0	0	0	0.0139(7)
Cd1	4*f*	1/3	2/3	0.6277(1)	0.0198(8)
Cd2[b]	6*h*	0.266(2)	0.533(3)	1/4	0.046(3)
As1	4*f*	1/3	2/3	0.0790(2)	0.0138(9)
As2[b]	6*h*	0.600(2)	0.201(3)	1/4	0.023(2)
		$PrCd_3As_3$			
Pr	2*a*	0	0	0	0.0129(6)
Cd1	4*f*	1/3	2/3	0.6275(1)	0.0187(7)
Cd2[b]	6*h*	0.267(2)	0.534(3)	1/4	0.047(3)
As1	4*f*	1/3	2/3	0.0783(2)	0.0127(8)
As2[b]	6*h*	0.602(2)	0.204(3)	1/4	0.022(2)

[a] U_{eq} is defined as one-third of the trace of the orthogonalized U_{ij} tensor. [b] Occupancies of 1/3.

of formula units per cell ("$LaZn_3As_3$", $Z = 4$) as in the orthorhombic model. The hexagonal model is based on a hypothetical $ScAl_3C_3$-type structure in which the cell parameters ($a = 4.185$ Å, $c = 20.510$ Å) were extrapolated linearly from the trend seen for $REZn_3As_3$ (RE = Ce−Nd, Sm; Table 1), and the atomic positions were taken from the crystal structure of $PrZn_3As_3$ (Table 3) but with Zn2 and As2 placed in idealized 2*c* (1/3, 2/3, 1/4) and 2*d* sites (1/3, 2/3, 3/4), respectively. The unit cell has roughly half the volume of those of the previous two models and contains two formula units of "$LaZn_3As_3$". The basis sets consisted of La 6s/6p/5d/4f, Zn 4s/4p/3d, and As 4s/4p/3d orbitals, with the La 6p and As 4d orbitals being downfolded. Integrations in reciprocal space were carried out with an improved tetrahedron method over appropriate *k*-point meshes (6 × 18 × 6 for orthorhombic, 12 × 12 × 4 for trigonal, and 12 × 12 × 4 for hexagonal models).

Table 4. Selected Interatomic Distances (Å) in $LaZn_3As_3$

La−As1 (×2)	3.0541(3)	Zn2−As1	2.4707(5)
La−As2 (×2)	3.1201(3)	Zn2−As2 (×2)	2.4723(3)
La−As1	3.1708(4)	Zn2−As3	2.7588(6)
La−As3 (×2)	3.2301(3)	Zn3−As1 (×2)	2.5047(3)
Zn1−As2	2.5346(5)	Zn3−As2	2.5298(5)
Zn1−As3 (×2)	2.5499(3)	Zn3−As3	2.5546(5)
Zn1−As3	2.6216(6)	Zn1−Zn1 (×2)	2.8065(6)

Table 5. Selected Interatomic Distances (Å) in $REZn_3As_3$ (RE = Pr, Nd, Sm) and $RECd_3As_3$ (RE = La−Pr)

	$PrZn_3As_3$	$NdZn_3As_3$	$SmZn_3As_3$
RE−As1 (×6)	2.995(2)	2.985(2)	2.961(2)
Zn1−As2	2.482(5)	2.484(5)	2.483(5)
Zn1−As1 (×3)	2.569(2)	2.567(2)	2.563(2)
Zn2−As2	2.397(19)	2.399(10)	2.384(10)
Zn2−As2	2.414(9)	2.42(2)	2.42(2)
Zn2−As2	2.549(9)	2.535(9)	2.517(9)
Zn2−As1 (×2)	3.372(4)	3.372(4)	3.384(4)
	$LaCd_3As_3$	$CeCd_3As_3$	$PrCd_3As_3$
RE−As1 (×6)	3.077(2)	3.052(2)	3.035(2)
Cd1−As2	2.660(4)	2.659(4)	2.656(3)
Cd1−As1 (×3)	2.752(2)	2.748(2)	2.744(2)
Cd2−As2	2.547(9)	2.541(9)	2.529(9)
Cd2−As2	2.56(2)	2.55(2)	2.55(2)
Cd2−As2	2.700(10)	2.688(10)	2.672(10)
Cd2−As1 (×2)	3.677(4)	3.686(4)	3.693(4)

RESULTS AND DISCUSSION

The phases previously known within the ternary RE−Zn−As systems can be divided into those containing early trivalent ($REZn_{0.67}As_2$ with defect tetragonal $SrZnBi_2$- or $HfCuSi_2$-type structures[4,5] and $RE_{0.67}Zn_2As_2$ with defect trigonal $CaAl_2Si_2$-type structures;[8] both series for RE = La−Nd, Sm) versus divalent rare-earth metals ($REZn_2As_2$ with $CaAl_2Si_2$-type structures for RE = Eu and Yb[26−28] and $Eu_{11}Zn_6As_{12}$ with a $Sr_{11}Cd_6Sb_{12}$-type structure[29]). The known ternary RE−Cd−As phases were limited only to two containing divalent rare-earth metals ($RECd_2As_2$ with $CaAl_2Si_2$-type structures for RE = Eu, Yb).[30] The series of arsenides presented here consist of $LaZn_3As_3$ with a new orthorhombic structure type and $REZn_3As_3$ (RE = Ce−Nd, Sm) and $RECd_3As_3$ (RE = La−Pr) with hexagonal $ScAl_3C_3$-type structures.

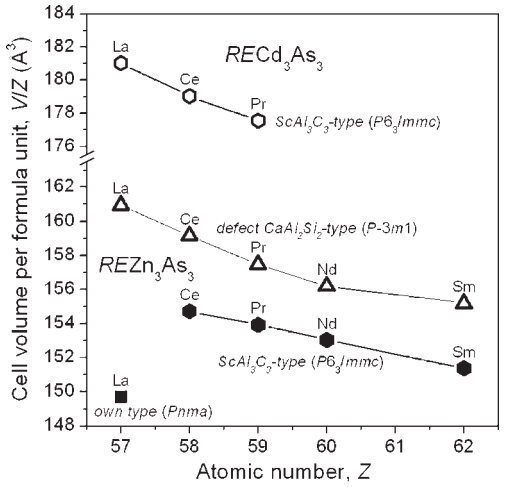

Figure 1. Plot of unit cell volumes per formula unit for ternary arsenides $REZn_3As_3$ and $RECd_3As_3$. Volumes for $RE_{0.67}Zn_2As_2$ with defect $CaAl_2Si_2$-type (taken from ref 8) are normalized to the formula "$REZn_3As_3$".

The composition of the phases $RE_{0.67}Zn_2As_2$ (defect $CaAl_2Si_2$-type) reported by Nientiedt et al.,[8] when multiplied by 3/2, corresponds to $REZn_3As_3$. That is, it becomes evident that there are several polymorphic modifications of $REZn_3As_3$. Interestingly, the conditions for the preparation of these compounds involved identical reaction stoichiometries (RE/Zn/As = 1:3:3) and identical annealing treatments (800 °C for 1 week). The critical points of departure in the syntheses are that we added either I_2 as a mineralizing agent or nothing extra, obtaining single-crystal or powder samples, respectively, of $LaZn_3As_3$- or $ScAl_3C_3$-type phases, whereas Nientiedt et al. added a NaCl/KCl flux, obtaining single-crystal samples of defect $CaAl_2Si_2$-type phases.[8] To rule out the possibility that a final slow-cooling step (from 800 °C to room temperature over 2 days) applied in our syntheses may have provoked a phase transformation, we repeated the direct reactions of the elements at 800 °C in the absence of I_2 but followed by quenching in cold water, with the same results. Lowering the annealing temperature to 650 °C followed by quenching also gave no change. On balance, the experimental evidence suggests that the thermodynamically stable polymorphs at 800 °C are the $LaZn_3As_3$- or $ScAl_3C_3$-type phases, whereas the defect $CaAl_2Si_2$-type phases are metastable forms that result from the use of the salt flux. Further work is in progress to elucidate the variables controlling the formation of these phases.

The unit cell volumes, normalized to the formula unit "REM_3As_3", generally follow the trends expected from the gradual decrease in radii on proceeding to the heavier RE metals (Figure 1). For $REZn_3As_3$, the hexagonal $ScAl_3C_3$-type polymorphs have smaller cell volumes per formula unit (for a given RE) and thus higher densities than the corresponding defect trigonal $CaAl_2Si_2$-type polymorphs, for which the RE sites are only partially occupied. This observation suggests that the $ScAl_3C_3$-type forms are stabilized at lower temperatures and higher pressures relative to the defect $CaAl_2Si_2$-type forms. Orthorhombic $LaZn_3As_3$ (own type) is remarkable for its anomalously small cell volume per formula unit. The efficient atom packing is readily apparent in its crystal structure, in which Zn-centered tetrahedra are linked to form a three-dimensional anionic framework $[Zn_3As_3]^{3-}$ delineating large channels running along the *b* direction that are occupied by

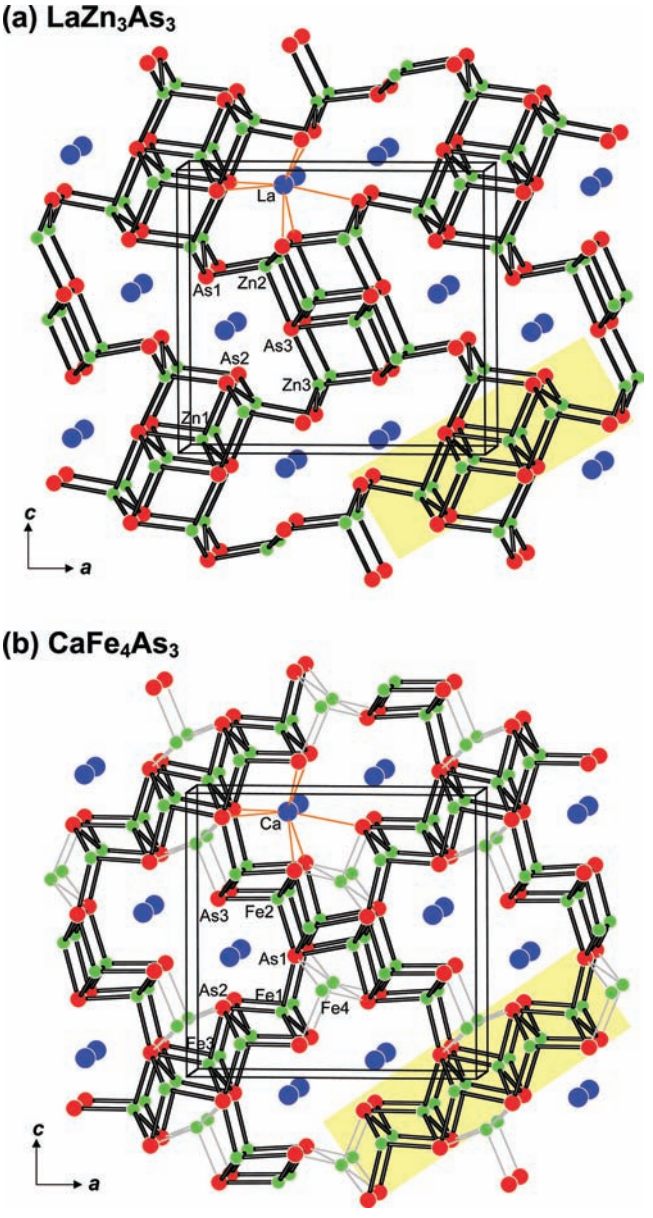

Figure 2. Structures of (a) orthorhombic $LaZn_3As_3$ and (b) $CaFe_4As_3$, viewed down the *b* direction. The large blue circles are La or Ca atoms. The small green circles are Zn or Fe atoms. The medium red circles are As atoms. Bonds within the Fe4-centered square pyramids in $CaFe_4As_3$ are shown in light gray. The PbO-type fragments are highlighted in yellow. The monocapped trigonal prismatic coordination environments (CN7) around the La or Ca atoms are highlighted with orange lines.

La^{3+} cations in monocapped trigonal prismatic coordination (Figure 2a). Although $LaZn_3As_3$ is isoelectronic to $BaCuZn_3As_3$,[31] which has similar cell parameters but crystallizes in space group *Cmcm*, they do not closely resemble each other. Instead, $LaZn_3As_3$ bears striking similarities to $CaFe_4As_3$ (Figure 2b), a recently discovered strongly correlated electron material exhibiting anisotropic physical properties and spin density waves.[9−11] Crystallizing in space group *Pnma* with similar cell parameters, both $LaZn_3As_3$ and $CaFe_4As_3$ can be considered to be constructed from crisscrossing ribbons (highlighted in yellow in Figure 2) that are fragments of the [MAs] layers so prevalent in other transition-metal pnictide structures, including superconducting arsenides

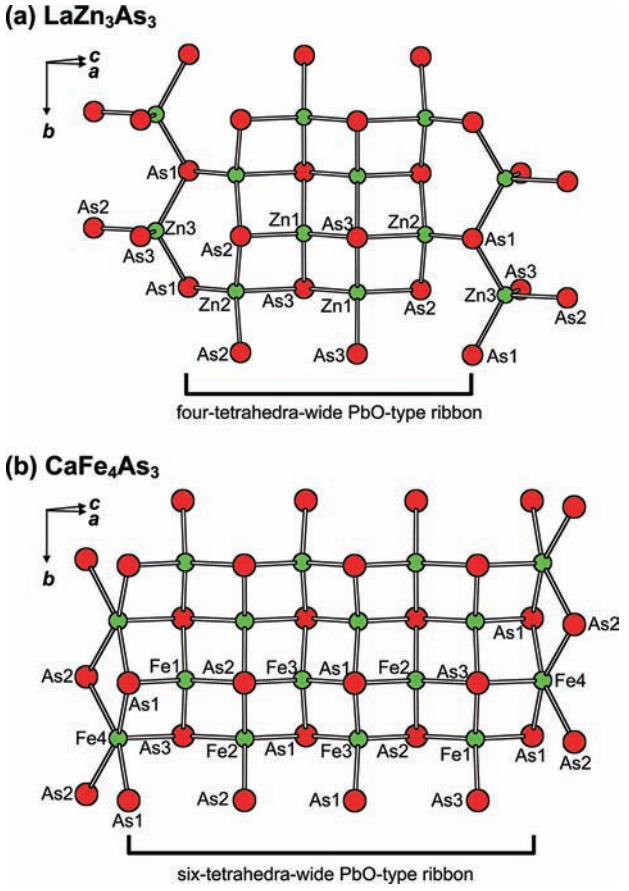

Figure 3. Comparison of PbO-type ribbons extending along the *b* direction in (a) orthorhombic $LaZn_3As_3$ and (b) $CaFe_4As_3$.

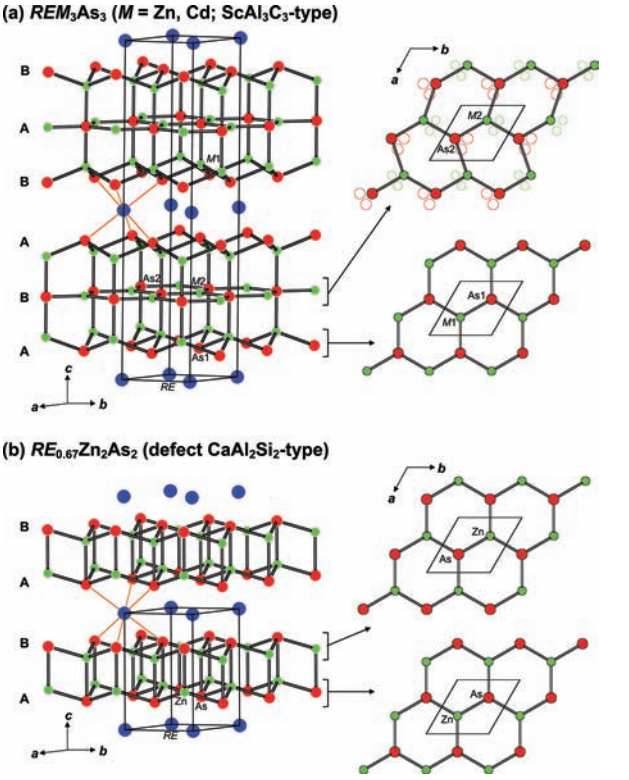

Figure 4. Comparison of (a) hexagonal $ScAl_3C_3$-type structure, adopted by $REZn_3As_3$ (RE = Ce−Nd, Sm) and $RECd_3As_3$ (RE = La−Pr) and (b) trigonal defect $CaAl_2Si_2$-type structure, adopted by $RE_{0.67}Zn_2As_2$ (RE = La−Nd, Sm). The large blue circles are RE atoms. The small green circles are Zn or Cd atoms. The medium red circles are As atoms. The octahedral coordination environments (CN6) around the RE atoms are highlighted with orange lines. In a, one of several possible local atomic arrangements is shown for the partially occupied M2 and As2 sites within the flat net at $z = 1/4$ (or 3/4). The labels **A** and **B** identify different orientations of close-packed layers of As atoms *alone*.

such as $BaFe_2As_2$ and LaFeAsO.[1,2] Metal-centered tetrahedra share their edges in a PbO-type arrangement to form these ribbons (or one-dimensional strips) that extend along the *b* direction and are either four-tetrahedra-wide (in $LaZn_3As_3$) or six-tetrahedra-wide (in $CaFe_4As_3$) (Figure 3). The ribbons are decorated on their sides by corner-sharing $ZnAs_4$ tetrahedra (in $LaZn_3As_3$) or edge-sharing $FeAs_5$ square pyramids (in $CaFe_4As_3$). The crisscrossing four-tetrahedra-wide ribbons must be connected by the Zn3-centered tetrahedra to form the three-dimensional framework in $LaZn_3As_3$; in contrast, the six-tetrahedra-wide ribbons are already connected directly in $CaFe_4As_3$, and the Fe4-centered square pyramids serve as additional linkers.

Hexagonal $REZn_3As_3$ (RE = Ce−Nd, Sm) and $RECd_3As_3$ (RE = La−Pr) have less dense structures than orthorhombic $LaZn_3As_3$. This may seem counterintuitive until one notes the preference of the larger La atom for the higher coordination number (CN7) supported in $LaZn_3As_3$, versus the lower coordination numbers (CN6) for the smaller RE atoms in the $ScAl_3C_3$-type structure adopted by the other compounds. The hexagonal structure also possesses a more open framework resulting from the all-corner-sharing connectivity of the Zn- or Cd-centered polyhedra. This structure type is rare: $REAl_3C_3$, $REZn_3P_3$, and $PrCd_3P_3$ were the only previously known examples,[16−20] and the compounds presented here are the first arsenide representatives. Two-dimensional slabs $[M_3As_3]^{3-}$, constructed from corner-sharing M1-centered tetrahedra and M2-centered trigonal planes, are stacked along the *c* direction and separated by the RE^{3+} cations in octahedral coordination (Figure 4a). Each $[M_3As_3]^{3-}$ slab consists of double layers of corner-sharing tetrahedra with coplanar bases; all "down"-pointing tetrahedra in the upper layer share common corners with corresponding "up"-pointing tetrahedra in the lower layer. The double layers can also be regarded as a stack of three heteroatomic honeycomb nets "MAs" (reminiscent of hexagonal BN), the two outer ones being puckered with six-membered rings in a chair conformation, and the inner one being flat. This is an idealization based on an undistorted $ScAl_3C_3$-type structure. In reality, all $ScAl_3C_3$-type representatives exhibit in-plane and out-of-plane displacements, often significant, of the atoms within the middle hexagonal net.[16−20] In the structures determined here, the M2 and As2 atoms were shifted from the ideal 2*c* and 2*d* sites (with $6\bar{m}2$ symmetry), respectively, in space group $P6_3/mmc$, to 6*h* sites (*mm*2 symmetry) at a partial occupancy of 1/3. Within constraints of reasonable Zn2−As2 (2.4−2.6 Å) or Cd2−As2 distances (2.5−2.7 Å), it is possible to envision local atomic arrangements in which angles of nearly 120° are still retained, as well as more distorted arrangements (top right of Figure 4a). The displacement ellipsoids of the M2 atoms are always elongated along the *c* direction; this feature likely reflects true dynamic motion that would be consistent with the unusually low coordination environment around these atoms, with only three neighboring

As atoms in the trigonal plane but with two axial As atoms far too distant (>3.3 Å in $REZn_3As_3$ or >3.6 Å in $RECd_3As_3$) to be interacting.

Close structural relationships can be drawn between hexagonal REM_3As_3 (M = Zn, Cd; $ScAl_3C_3$-type) and trigonal $RE_{0.67}Zn_2As_2$ (defect $CaAl_2Si_2$-type; Figure 4b),[8] the latter having the same formula if multiplied by 3/2, as noted earlier. Both structures can be built up of the heteroatomic honeycomb nets "MAs" described above, interspersed with hexagonal RE nets of half the atomic density. The chemical formulas are then easily related to these nets: hexagonal REM_3As_3 consists of three "MAs" nets followed by one RE net, whereas trigonal $RE_{0.67}Zn_2As_2$ has two "MAs" nets followed by one RE net in which the sites are 67% occupied. It is also possible to describe these structures in terms of the stacking of close-packed layers of atoms, as Nientiedt et al. have done for $PrCd_3P_3$, with smaller P atoms occupying interstitial sites between close-packed layers of larger Pr and Cd atoms.[17] Alternatively, it may be informative to return to the more usual approach of considering the *anions* to be in close-packed layers and placing the *cations* in interstitial sites, if an ionic picture is assumed, however unrealistic it may be. Thought of in this manner, the structures of hexagonal REM_3As_3 and trigonal $RE_{0.67}Zn_2As_2$ are built up from an *identical* stacking sequence (ABAB...) of layers of close-packed As atoms (Figure 4). In hexagonal REM_3As_3, M atoms enter half of the available tetrahedral sites between adjacent close-packed As layers in the three-layer repeat units ABA or BAB, and RE atoms enter the octahedral sites between these latter units. Additional M atoms also enter the trigonal planar sites coplanar with the middle layers of these repeat units. (A curious relationship, which to our knowledge has not been noted previously, that emerges from this analysis is that covellite, a form of CuS and a naturally occurring superconductor,[21−23,32] is also constructed from similar three-layer units of S anions but arranged in the sequence (ABA)(ACA) with S−S bonds between these units.) In trigonal $RE_{0.67}Zn_2As_2$, Zn atoms enter all of the tetrahedral sites between every other pair of close-packed As layers, and RE atoms enter 67% of the octahedral sites between the remaining pairs of layers. With this insight, it is likely that the particular stacking sequence and occupation of interstitial sites would be sensitive to synthesis conditions that might favor the nucleation of one polymorph over another. Indeed, the cell parameters within the *ab* plane are similar (cf., a = 4.1772(7) Å for hexagonal $CeZn_3As_3$ vs a = 4.1717(6) Å for trigonal $Ce_{0.67}Zn_2As_2$),[8] and it is possible to envision that intergrowths of the two structure types might readily form.

Bond distances in these new arsenides are generally normal (Tables 4 and 5). The average RE−As distances tend to shorten, in accordance with expectations, as the coordination number around the RE atom becomes lower; for example, the average La−As distances decrease from 3.140(1) Å in orthorhombic $LaZn_3As_3$ (CN7) to 3.077(2) Å in hexagonal $LaCd_3As_3$ (CN6). As reflected by the range in Zn−As distances, the Zn-centered tetrahedra tend to show more distortion in orthorhombic $LaZn_3As_3$ (2.5047(3)−2.7588(6) Å) than in hexagonal $REZn_3As_3$ structures (2.482(5)−2.569(2) Å). These distances are similar to those in other structures where $ZnAs_4$ tetrahedra are found (e.g., 2.5629(7) Å in $LaZn_{0.67}As_2$, 2.526(1)−2.624(1) Å in $Ce_{0.63}Zn_2As_2$, and 2.455(1)−2.575(1) Å in $Eu_{11}Zn_6As_{12}$).[5,8,29] In contrast, the Zn−As distances within the Zn-centered trigonal planes in the hexagonal $REZn_3As_3$ structures are quite short (e.g., 2.38(1)−2.52(1) Å in $SmZn_3As_3$) relative to the sum of the

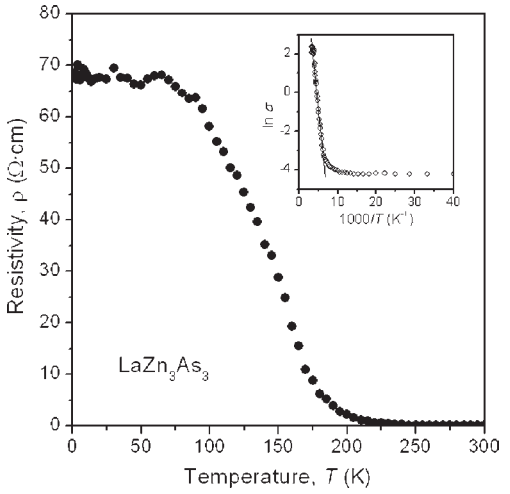

Figure 5. Plot of electrical resistivity vs temperature for orthorhombic $LaZn_3As_3$. The inset shows a plot of the natural logarithm of the electrical conductivity vs inverse temperature.

Pauling metallic radii ($r_{Zn} + r_{As}$ = 1.213 Å + 1.210 Å = 2.423 Å),[33] although distances as short as 2.36(1) Å are present in Zn_3As_2.[12] Corner-sharing Zn-centered trigonal planes, with Zn−As distances of 2.442(1) Å, are also found in KZnAs,[34] building up flat nets similar to those in hexagonal $REZn_3As_3$. In $RECd_3As_3$, the Cd−As distances in the Cd-centered tetrahedra (2.656(3)−2.752(2) Å) are intermediate between the sum of the Pauling radii ($r_{Cd} + r_{As}$ = 1.382 Å + 1.210 Å = 2.592 Å)[33] and corresponding values in $Ba_2Cd_2As_3$ (2.7151(6)−2.9093(7) Å),[35] whereas the distances in the Cd-centered trigonal planes (2.53(1)−2.70(1) Å) are again unusually short (cf., 2.51(3)−3.20(3) Å in Cd_3As_2).[13,14] There are no close metal−metal contacts in the hexagonal $REZn_3As_3$ and $RECd_3As_3$ structures. However, orthorhombic $LaZn_3As_3$ does contain Zn1−Zn1 distances of 2.8065(6) Å within the four-tetrahedra-wide ribbons that are fragments of related [ZnAs] layers found in $LaZn_{0.67}As_2$ (defect $SrZnBi_2$-type),[5] where the Zn−Zn distances are 2.8829(6) Å and weak metal−metal bonding is implicated.

The formulas $REZn_3As_3$ and $RECd_3As_3$ are charge-balanced. In accordance with the Zintl−Klemm concept, the electron-precise formulations $(RE^{3+})(Zn^{2+})_3(As^{3-})_3$ and $(RE^{3+})(Cd^{2+})_3(As^{3-})_3$ imply closed-shell electron configurations and the absence of As−As bonding. These requirements, of course, do not restrict the many different ways that Zn- or Cd-centered polyhedra can be linked together to build the crystal structures. However, all polymorphs observed would be expected to have band gaps in their electronic structures. In agreement with this prediction, a preliminary measurement of the electrical resistivity of orthorhombic $LaZn_3As_3$ reveals thermally activated behavior suggestive of a semiconductor (Figure 5). With the assumption that the behavior above 100 K is beyond the exhaustion regime, fitting the high-temperature portion to $\ln \sigma = \ln \sigma_0 - (E_g/2kT)$ (inset of Figure 5) gives an intrinsic band gap of 0.32 eV. The magnetic behavior of $LaZn_3As_3$ is unremarkable, with a small, positive temperature-independent susceptibility (~0.0005 emu/mol) superimposed by a significant Curie tail at low temperatures arising from magnetic impurities in the sample (Figure S4 in Supporting Information). Plots of the temperature dependence of the magnetic susceptibility for $REZn_3As_3$ (RE = Ce, Pr, Nd) are shown in Figure 6. The inverse susceptibility curve for $CeZn_3As_3$

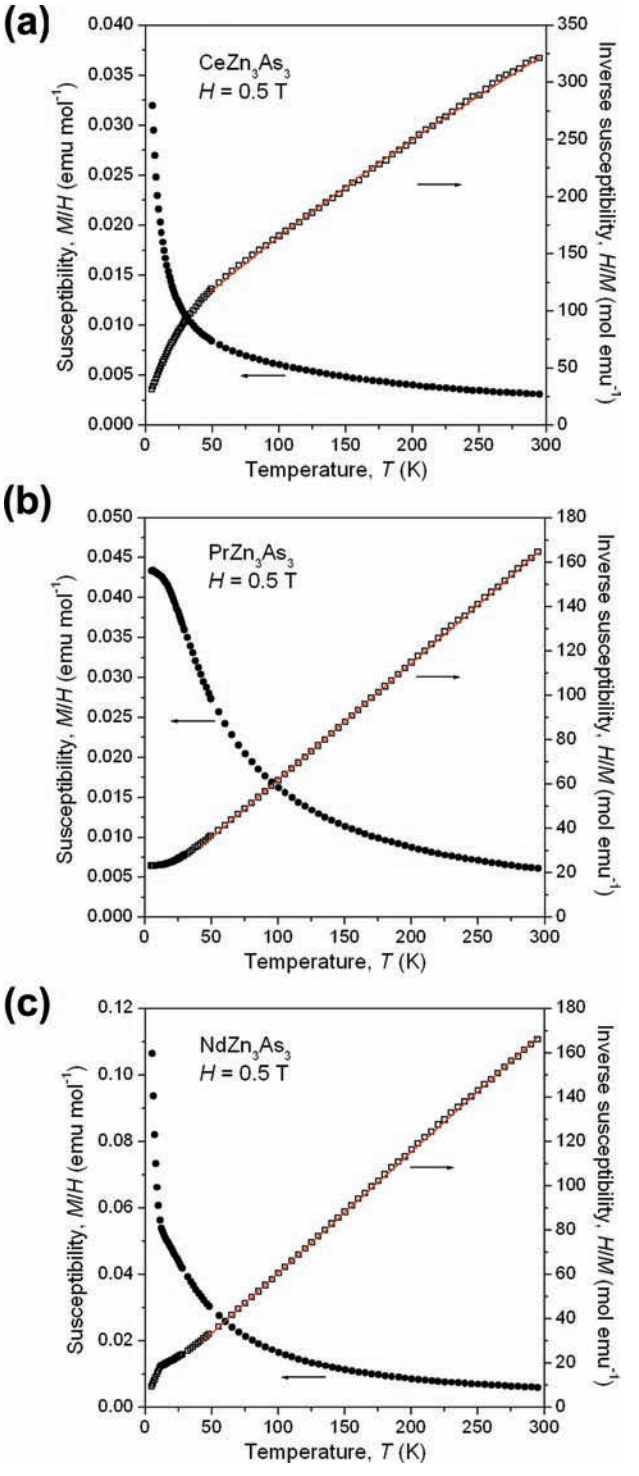

Figure 6. Plots of magnetic susceptibility (and its inverse) vs temperature for $REZn_3As_3$ (RE = Ce, Pr, Nd).

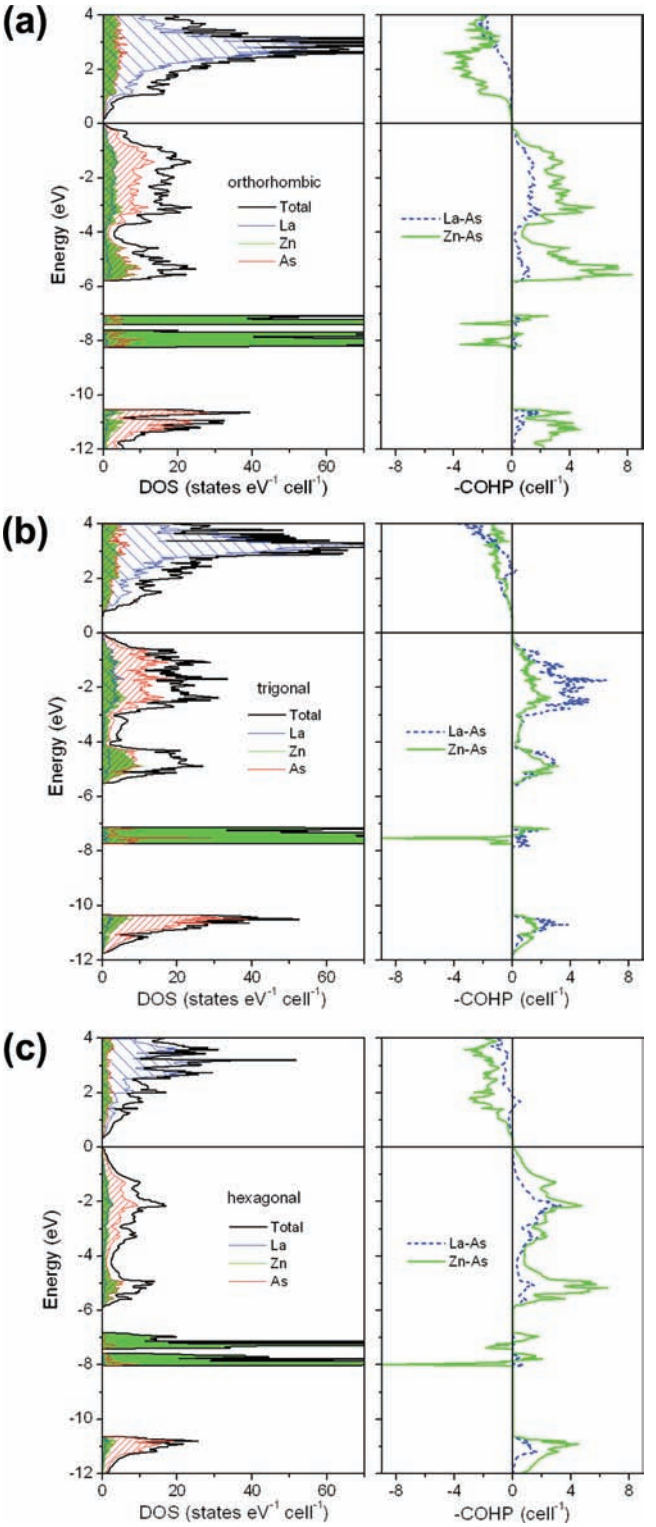

Figure 7. Band structures of (a) orthorhombic, (b) trigonal, and (c) hexagonal models of $LaZn_3As_3$, as detailed in the text. The left panels show the density of states (DOS) and their La (sparsely hatched blue regions), Zn (filled green regions), and As (densely hatched red regions) projections. The right panels show the crystal orbital Hamilton population (−COHP) curves for La−As (dashed blue lines) and Zn−As (solid green lines) contacts. The horizontal line at 0 eV marks the Fermi level.

is slightly convex; fitting of the region from 50 to 300 K to the modified Curie−Weiss law, $\chi = C/(T - \theta_p) + \chi_0$, yielded parameters of $C = 0.88(2)$ mol/emu·K, $\theta_p = -62(2)$ K, and $\chi_0 = 0.0006(1)$ emu/mol. The inverse susceptibility curves for $PrZn_3As_3$ and $NdZn_3As_3$ are relatively linear with temperatures above 50 K; they could be fit to the normal Curie−Weiss law, $\chi = C/(T - \theta_p)$, yielding parameters of $C = 1.91(1)$ mol/emu·K and $\theta_p = -18(1)$ K for $PrZn_3As_3$ and $C = 1.83(1)$ mol/emu·K and $\theta_p = -11(1)$ K for $NdZn_3As_3$. The effective magnetic moments

dx.doi.org/10.1021/ic201708x |*Inorg. Chem.* 2011, 50, 11152–11161

Table 6. Comparison of Calculated Electronic Structures of $LaZn_3As_3$ in Different Models

model	orthorhombic ($LaZn_3As_3$-type)	trigonal (defect $CaAl_2Si_2$-type superstructure)	hexagonal ($ScAl_3C_3$-type)
ΔE (kJ mol^{-1}) [a]	96	69	0
E_g (eV)	0.15	0.51	0.26
avg −ICOHP (eV bond^{-1})			
La−As	0.86	1.01	0.97
Zn−As	1.62	1.71	2.00
Zn−Zn	0.33	0.20	

[a] Relative to hexagonal model.

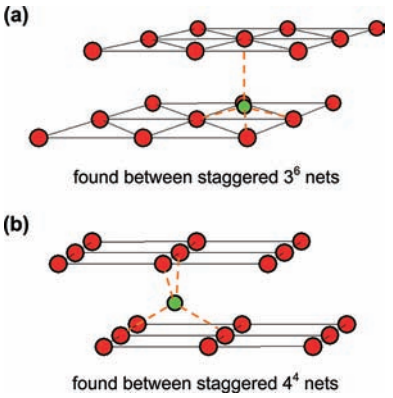

Figure 8. The generation of tetrahedral sites, occupied by Zn atoms, between pairs of staggered (a) triangular (3^6) or (b) square (4^4) nets of As atoms found in structural fragments of several ternary RE−Zn−As phases.

μ_{eff} derived from the Curie constants are 2.65(3), 3.90(1), and 3.83(1) μ_B for the Ce, Pr, and Nd compounds, respectively. These values are slightly larger than expected for the trivalent RE free ions (Ce^{3+}, 2.54 μ_B; Pr^{3+}, 3.58 μ_B; Nd^{3+}, 3.62 μ_B), possibly because of the presence of magnetic impurities at a level not detectable in the XRD patterns. The negative Weiss constants suggest antiferromagnetic exchange interactions, but further measurements of the electrical and magnetic properties of these and the other arsenides are required for more detailed interpretation.

The presence of a band gap is corroborated in electronic structure calculations for $LaZn_3As_3$ in three models: the orthorhombic structure reported here (own type), an ordered superstructure of the defect trigonal $CaAl_2Si_2$-type observed previously ($La_{0.67}Zn_2As_2$),[8] and a hypothetical hexagonal $ScAl_3C_3$-type structure. The density of states (DOS) and crystal orbital Hamilton population (COHP) curves are shown in Figure 7, and some numerical results are summarized in Table 6. The band gap is the smallest in the orthorhombic model (0.15 eV, in fair agreement with the experimental value) and largest in the trigonal model (0.51 eV). The DOS curves in all three models show mostly empty La-based states above the Fermi level and mostly filled Zn- and As-based states below, in agreement with the simple formulations based on the Zintl−Klemm concept. Essentially all of the Zn 3d states are localized within the sharp spike in the DOS between −7 and −8 eV. The most important contributions to covalent bonding are the Zn−As interactions, with all bonding levels (from −6 to 0 eV) and no antibonding levels filled up to the Fermi level, followed by the La−As interactions. The Zn−Zn interactions (not shown in the COHP curves) corresponding to the 2.81 Å (orthorhombic model) or the longer 3.06 Å distances (trigonal model) have very low −ICOHP values and can be regarded as negligibly weak. It is a little puzzling that the model with the lowest total energy is the unobserved hexagonal $ScAl_3C_3$-type, whereas the model with the highest total energy is the experimentally observed orthorhombic one. However, these models have not been structurally optimized with computational methods, and a proper comparison may require further investigation. Moreover, we have not considered electrostatic interactions (Madelung energy), which will surely contribute to additional stabilization through ionic bonding.

CONCLUSIONS

The ternary rare-earth arsenides $REZn_3As_3$ and $RECd_3As_3$ exhibit a rich structural chemistry that is manifested by the formation of several polymorphs. For $REZn_3As_3$, three structure types with orthorhombic, hexagonal, and trigonal symmetry are found, depending on the identity of the RE metal and the synthesis conditions. Many of the key structural features in these and other ternary RE−Zn−As phases can be understood in terms of two basic arrangements of Zn-centered tetrahedra, which can be derived from filling the sites between staggered triangular (3^6) or square nets (4^4) of As atoms (Figure 8). The triangular arrangements are found in the layers in $REZn_3As_3$ ($ScAl_3C_3$-type) and $RE_{0.67}Zn_2As_2$ (defect $CaAl_2Si_2$-type),[8] whereas the square arrangements are found in layers in $REZn_{1-x}As_2$ (defect $SrZnBi_2$- or $HfCuSi_2$-type)[4,5] or in fragments in $LaZn_3As_3$ (own type). In addition, metal atoms enter trigonal planar sites in the $ScAl_3C_3$-type structure of hexagonal $REZn_3As_3$ and $RECd_3As_3$. The occurrence of three-coordinate Zn and Cd is unusual, but known in some molecular complexes where it must be supported through the use of bulky ligands.[36−38] Trigonal planar $ZnAs_3$ and $CdAs_3$ units are rarely found in solid-state extended structures.[34] These arsenides are predicted to be small band gap semiconductors. The resemblance of orthorhombic $LaZn_3As_3$ to $CaFe_4As_3$ suggests possibilities for chemical substitution to change the electron count that might render it metallic. The disorder and large thermal motion experienced by the three-coordinate Zn or Cd atoms in the $ScAl_3C_3$-type phases also suggest that the thermal transport properties may be worthwhile to investigate.

ASSOCIATED CONTENT

Supporting Information. X-ray crystallographic files in CIF format, additional tables of crystallographic data, powder XRD patterns, SEM images, and magnetic susceptibility of $LaZn_3As_3$. This material is available free of charge via the Internet at http://pubs.acs.org.

AUTHOR INFORMATION

Corresponding Author
*E-mail: arthur.mar@ualberta.ca.

ACKNOWLEDGMENT

The Natural Sciences and Engineering Research Council of Canada and the University of Alberta supported this work. We thank Dr. Robert McDonald (X-Ray Crystallography Laboratory) for some of the X-ray data collections and Ms. Christina Barker

(Department of Chemical and Materials Engineering) and Ms. De-Ann Rollings (Department of Earth and Atmospheric Sciences) for assistance with the EDX analysis. We thank Dr. Athena Safa-Sefat and Dr. Bayrammurad Saparov (Oak Ridge National Laboratory) for the magnetic susceptibility measurement of $LaZn_3As_3$.

REFERENCES

(1) Rotter, M.; Tegel, M.; Johrendt, D. *Phys. Rev. Lett.* **2008**, *101*, 107006−1–107006−4.
(2) Kamihara, Y.; Watanabe, T.; Hirano, M.; Hosono, H. *J. Am. Chem. Soc.* **2008**, *130*, 3296–3297.
(3) Stoyko, S. S.; Blanchard, P. E. R.; Mar, A. *Inorg. Chem.* **2010**, *49*, 2325–2333.
(4) Nientiedt, A. T.; Jeitschko, W. *J. Solid State Chem.* **1999**, *142*, 266–272.
(5) Stoyko, S. S.; Mar, A. *J. Solid State Chem.* **2011**, *184*, 2360−2367.
(6) Zelinska, O. Ya.; Mar, A. *J. Solid State Chem.* **2006**, *179*, 3776–3783.
(7) Zelinska, O. Ya.; Mar, A. *J. Alloys Compd.* **2008**, *451*, 606–609.
(8) Nientiedt, A. T.; Lincke, H.; Rodewald, U. Ch.; Pöttgen, R.; Jeitschko, W. *Z. Naturforsch., B: J. Chem. Sci.* **2011**, *66*, 221–226.
(9) Todorov, I.; Chung, D. Y.; Malliakas, C. D.; Li, Q.; Bakas, T.; Douvalis, A.; Trimarchi, G.; Gray, K.; Mitchell, J. F.; Freeman, A. J.; Kanatzidis, M. G. *J. Am. Chem. Soc.* **2009**, *131*, 5405–5407.
(10) Zhao, L. L.; Yi, T.; Fettinger, J. C.; Kauzlarich, S. M.; Morosan, E. *Phys. Rev. B* **2009**, *80*, 020404−1–020404−4.
(11) Todorov, I.; Chung, D. Y.; Claus, H.; Gray, K. E.; Li, Q.; Schleuter, J.; Bakas, T.; Douvalis, A. P.; Gutmann, M.; Kanatzidis, M. G. *Chem. Mater.* **2010**, *22*, 4996–5002.
(12) de Vries, G. C.; Frikkee, E.; Helmholdt, R. B.; Kopinga, K.; de Jonge, W. J. M. *Physica B* **1989**, *156&157*, 321–323.
(13) Steigmann, G. A.; Goodyear, J. *Acta Crystallogr., Sect. B: Struct. Crystallogr. Cryst. Chem.* **1968**, *24*, 1062–1067.
(14) Pietraszko, A.; Łukaszewicz, K. *Acta Crystallogr., Sect. B: Struct. Crystallogr. Cryst. Chem.* **1969**, *25*, 988–990.
(15) Sheldrick, G. M. *SHELXTL*, version 6.12; Bruker AXS Inc.: Madison, WI, 2001.
(16) Tsokol', A. O.; Bodak, O. I.; Marusin, E. P.; Baivel'man, M. G. *Sov. Phys. Crystallogr.* **1986**, *31*, 467–468. *Transl. Kristallografiya* **1986**, *31*, 791–792.
(17) Nientiedt, A. T.; Jeitschko, W. *J. Solid State Chem.* **1999**, *146*, 478–483.
(18) Gesing, T. M.; Pöttgen, R.; Jeitschko, W.; Wortmann, U. *J. Alloys Compd.* **1992**, *186*, 321–331.
(19) Gesing, T. M.; Jeitschko, W. *J. Solid State Chem.* **1998**, *140*, 396–401.
(20) Tejedor, P.; Hollander, F. J.; Fayos, J.; Stacy, A. M. *J. Cryst. Growth* **1995**, *155*, 223–228.
(21) Oftedal, I. *Z. Kristallogr., Kristallgeom., Kristallphys., Kristallchem.* **1932**, *83*, 9–25.
(22) Evans, H. T., Jr.; Konnert, J. A. *Am. Mineral.* **1976**, *61*, 996–1000.
(23) Ohmasa, M.; Suzuki, M.; Takeuchi, Y. *Mineral. J.* **1977**, *8*, 311–319.
(24) Gelato, L. M.; Parthé, E. *J. Appl. Crystallogr.* **1987**, *20*, 139–143.
(25) Tank, R.; Jepsen, O.; Burkhardt, A.; Andersen, O. K. *TB-LMTO-ASA Program*, version 4.7; Max Planck Institut für Festkörperforschung: Stuttgart, Germany, 1998.
(26) Klüfers, P.; Neumann, H.; Mewis, A.; Schuster, H.-U. *Z. Naturforsch., B: Anorg. Chem., Org. Chem.* **1980**, *35*, 1317–1318.
(27) Zwiener, G.; Neumann, H.; Schuster, H.-U. *Z. Naturforsch., B: Anorg. Chem., Org. Chem.* **1981**, *36*, 1195–1197.
(28) Nateprov, A.; Cisowski, J.; Heimann, J.; Mirebeau, I. *J. Alloys Compd.* **1999**, *290*, 6–9.
(29) Saparov, B.; Bobev, S. *Acta Crystallogr., Sect. E: Struct. Rep. Online* **2010**, *66*, i24.
(30) Artmann, A.; Mewis, A.; Roepke, M.; Michels, G. *Z. Anorg. Allg. Chem.* **1996**, *622*, 679–682.
(31) Ozawa, T. C.; Kauzlarich, S. M. *Inorg. Chem.* **2003**, *42*, 3183–3186.
(32) di Benedetto, F.; Borgheresi, M.; Caneschi, A.; Chastanet, G.; Cipriani, C.; Gatteschi, D.; Pratesi, G.; Romanelli, M.; Sessoli, R. *Eur. J. Mineral.* **2006**, *18*, 283–287.
(33) Pauling, L. *The Nature of the Chemical Bond*, 3rd ed.; Cornell University Press: Ithaca, NY, 1960.
(34) Vogel, R.; Schuster, H.-U. *Z. Naturforsch., B: Anorg. Chem., Org. Chem.* **1980**, *35*, 114–116.
(35) Saparov, B.; He, H.; Zhang, X.; Greene, R.; Bobev, S. *Dalton Trans.* **2010**, *39*, 1063–1070.
(36) Gruff, E. S.; Koch, S. A. *J. Am. Chem. Soc.* **1990**, *112*, 1245–1247.
(37) Thiele, K.; Görls, H.; Seidel, W. *Z. Anorg. Allg. Chem.* **1998**, *624*, 555–556.
(38) Darensbourg, D. J.; Niezgoda, S. A.; Draper, J. D.; Reibenspies, J. H. *Inorg. Chem.* **1999**, *38*, 1356–1359.